

Facilitating Push-Off Propulsion: A Biomechanical Model Of Ankle Robotics Assistance For Plantarflexion Gait Training In Stroke

Anindo Roy, *Senior Member, IEEE*, Hermano I. Krebs, *Fellow, IEEE*,
Kamran Iqbal, *Senior Member, IEEE*, Nathan R. Macko, *Student Member, IEEE*,
Richard F. Macko, and Larry W. Forrester

Abstract—Individuals with stroke often have diminished muscle strength that contributes to impaired push-off propulsion during walking, resulting in abnormal compensatory mechanisms and slower gait speeds. In this paper, we present a sagittal, 2-link biomechanical model of ankle push-off propulsion dynamics. The purpose of the model is to predict the parameters of an impedance controller to generate a desired level of anterior-posterior push-off during assisted walking with a modular ankle robot (“Anklebot”). In conjunction with our development of a novel gait event-triggered training approach, this model will facilitate tailoring the assisted push-off to individual severity. Here, we develop the model from first principles and experimentally validate it in a healthy subject.

I. INTRODUCTION

THE ability to walk and maintain balance is essential for successful and safe execution of activities of daily life (ADL). Following a stroke, the leading cause of long-term disability in the United States [1], the impact on walking is often significant, negatively affecting an individual’s mobility [2] at home and in the community.

Ambulation speed is widely used as a measure of functional recovery in post-stroke rehabilitation [3], and may be thought of as a “global” top-level outcome that is influenced by a multitude of spatio-temporal kinematic (e.g., cadence, cycle time, stance and swing duration, stride length) and kinetic (ground reaction forces [GRF], joint torques) variables. One such key contributor to walking

speed is the anterior-posterior (A-P) push-off propulsion during the mid-to-terminal stance (MTS) phase of gait [4]. Subjects with hemiparetic (HP) gait often generate less propulsion in the paretic leg compared to the non-paretic leg [5] that compromises economical gait and leads to slower walking speeds [6]. Hence, asymmetric paretic leg A-P propulsion has been a subject of numerous investigations (e.g., [4,5,7]) and has been correlated to gait function [7].

The US Department of Veterans Affairs Baltimore Medical Center (VAMC), in collaboration with MIT, has developed a modular, impedance-controlled, 2 active DOF actuated ankle robot (“Anklebot”) [8] to improve walking and balance functions after stroke, by means of increasing the paretic ankle contribution into task-oriented functional activities (Fig. 1). To date, our studies have demonstrated in different phases of stroke that seated visually-guided and evoked isolated ankle training with the Anklebot improves paretic ankle motor control (smoother, faster and more accurate ankle targeting) that translates to faster steady-state floor walking speeds [9] and improved gait symmetry [10]. Notably, the average gain (20%) in floor-walking speed after 6-week seated Anklebot training was comparable or greater than that reported in other task-specific, robotic gait training studies in chronic stroke (e.g. [11]). Here we expand beyond seated posture to integrate the Anklebot directly into task-specific locomotor training to examine whether perhaps we can further enhance gait function.

Toward that end, we have recently developed and are clinically testing a new gait event-triggered, deficit-adjusted

Manuscript received May 23, 2014. This work was funded by the Department of Veterans Affairs Rehabilitation Research and Development Service (VA RR&D) “Center of Excellence on Task-Oriented Exercise and Robotics in Neurological Diseases,” (B3688R) and VA RR&D Merit Pilot Award (A7461P).

A. Roy is with the Dept. of Neurology, University of Maryland School of Medicine (UMB-SOM) and the VA RR&D Maryland Exercise and Robotics Center of Excellence (MERCE), Baltimore, MD 21201 (phone: 410-637-3241; fax: 410-605-7913; e-mail: ARoy@som.umaryland.edu).

H.I. Krebs is with the Dept. of Mechanical Engineering, Massachusetts Institute of Technology (MIT), Cambridge, MA 02139 (e-mail: hikrebs@mit.edu).

K. Iqbal is with the Dept. of Mechanical and Aerospace Engineering, University of California at Irvine, Irvine, CA 92697 (email: iqbalk@uci.edu).

N.R. Macko is with the Dept. of Electrical and Computer Engineering, University of Maryland, College Park, MD 20742 (e-mail: nmacko@umd.edu).

R.F. Macko is with UMB-SOM Dept. of Neurology, the VA RR&D MERCE, and the Geriatric Research Education and Clinical Core, Baltimore, MD 21201 (email: rmacko@grecc.umaryland.edu).

L.W. Forrester is with UMB-SOM Dept. of Physical Therapy and Rehabilitation Science and the VA RR&D MERCE, Baltimore, MD 21201 (e-mail: LForrester@som.umaryland.edu).



Fig. 1. Stroke participant undergoing Anklebot-assisted gait training on a treadmill. The Anklebot is providing plantar flexion push-off at the paretic ankle during mid-to-terminal stance, beginning with heel-off and peaking just prior to toe-off.

control approach that incorporates offline sagittal-plane biomechanical models (specifically, for swing and landing phases), for using the Anklebot to train upright locomotion on a treadmill (TM) [12]. This novel approach seeks to optimize walking recovery based on profiles of biomechanical impediments in HP gait (e.g., foot drop vs. impaired push-off vs. poor landing) by precisely timing robotic support to gait phases (e.g., swing) that correspond to key HP deficits (e.g., foot drop). The biomechanical models described in [12] are used for initial parameterization of the Anklebot and for systematic progression of training parameters based on prior and ongoing performance. Initial findings from our ongoing TM-based Anklebot training study are very promising. In four chronic stroke subjects with dorsiflexion (DF) swing deficits¹ (peak swing [PSW]: $-2.7^{\circ} \pm 3.5^{\circ}$, mid swing [MSW]: $-3.8^{\circ} \pm 3.1^{\circ}$), six weeks (3x weekly) of TM-Anklebot training targeted to swing DF, led to robust and significant improvements in swing function (PSW: $+7.3^{\circ} \pm 4.7^{\circ}$, $\Delta=370\%$; MSW: $+4.8^{\circ} \pm 4.3^{\circ}$, $\Delta=226\%$). These gains were even greater at 6-week follow-up (PSW: $+8.4^{\circ} \pm 6.7^{\circ}$, MSW: $5.1^{\circ} \pm 7.3^{\circ}$). However, to our surprise, subjects also showed gains in plantar flexor push-off at 6 weeks (~3-fold increase in MTS A-P propulsive impulse) and this was retained with even higher values at 6 weeks post-completion (9.8 N-s to 17.8 N-s), even though this effect was not targeted. Notably, all 4 patients discarded use of their ankle brace at follow-up and anecdotal evidence suggests better independent ADL mobility function at home.

Motivated by these initial findings, we are further refining our control scheme [12] to incorporate a biomechanical model for A-P propulsion dynamics. Contrary to our upper-extremity adaptive algorithm [13], the Anklebot adaptive approach does not *auto*-modulate the controller gains or the commanded inputs in order to up- or down-regulate robotic outputs--e.g., amount or rate of assistance--to changes in performance--e.g., walking speed (presently adjusted manually based on therapists' observation and self-reported patient feedback). Here, we seek to address the 1st of these two issues by: 1) developing a sagittal-plane biomechanical model that links robotic support to paretic leg MTS A-P propulsive impulse across different walking speeds; and 2) validating the model in an able-bodied subject, as a 1st pass.

A. The problem: pathological push-off post stroke

In stroke, decreased paretic leg push-off propulsion has been attributed to a multitude of factors, such as: a) an inability to recruit agonist muscles responsible for generation of propulsion resulting in decreased paretic hip extension in late stance (LS) [5]; and b) increased antagonist muscle coactivation resulting in exaggerated flexor activity [5]. Thus the resultant interaction torques counteract plantar flexor output to cause premature offloading of the leg,

¹Swing function was characterized by paretic peak DF angle and mid swing angle during unassisted TM walking. Mid swing angle in particular, has special significance since the foot-floor local minima typically occurs at this time point. Hence, these measures are reasonable surrogates of foot-floor clearance or ground elevation during the swing phase.

thereby interfering with the ability to generate sufficient propulsion. These, and other deficits, contribute to inefficient, compensatory gait biomechanics: for example, increased paretic hip flexor activity that leads to dystrophic or circumduction gait—a phenomenon in which the paretic leg swings in a semicircle from medial to lateral direction during LS and into swing that advances the leg further, but in a manner that limits the posterior position of the paretic foot at push-off. Circumduction also results from hip “hike” and lateral lean arising from the paretic side. As a result, subjects have difficulty in stabilizing their pelvis as they walk—they hike their hip to elevate the paretic leg for dynamic body weight transfer and ground clearance.

B. Potential solution: gait event-triggered Anklebot therapy

We have developed a gait event-triggered control approach (US patent pending, #61/906,453) to time robotic support to gait events that correspond to key functional HP gait deficits (Fig. 2). The control approach has been previously described in detail [12]—here we recapitulate its basic working principle and key salient features. Briefly, the Anklebot delivers torques at the paretic ankle during one or more key time epochs, each with unique functional needs: (1) PF torque to enhance push-off propulsion during MTS, starting with heel-off and peaking just prior to toe-off; (2) DF torque to facilitate swing clearance during initial swing, starting at toe-off and continuing until mid-swing; and (3) Restorative viscous torque to lessen impact force at landing. Anklebot torque is generated by commanding a programmable positional reference trajectory. The impedance controller generates torques proportional to the magnitude of the positional and velocity error between the commanded and actual ankle position via the torsional stiffness (K) and damping (b) settings. The precise timing of robotic actuation to gait events is achieved via footswitch insoles that detect the occurrence of the specified events (Fig. 3). This enables “on-the fly” adjustment of robotic outputs across strides, thereby accounting for step-to-step variability by ensuring stability of the human-robot interface during assisted locomotor training that is critical for safety.

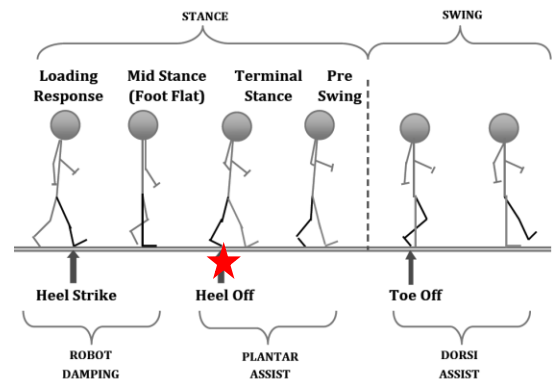


Fig. 2. Conceptual diagram showing three key events during a gait cycle. Depending on the type of gait deficit(s), the Anklebot is programmed to generate assistive (or resistive) torques at the paretic ankle during one or more gait events; in this case, PF assistance during mid-to-terminal stance for enhanced push-off propulsion (asterisk).

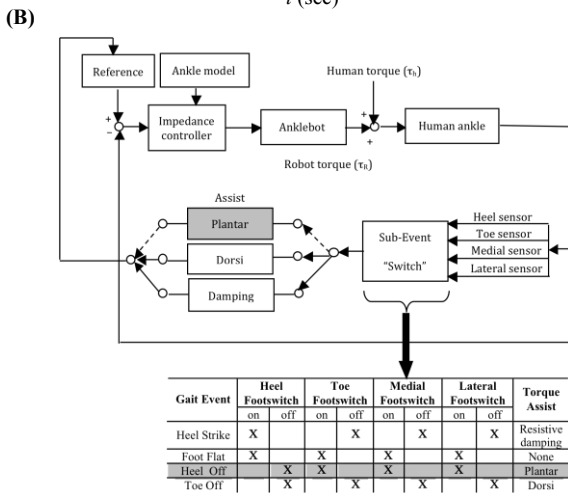
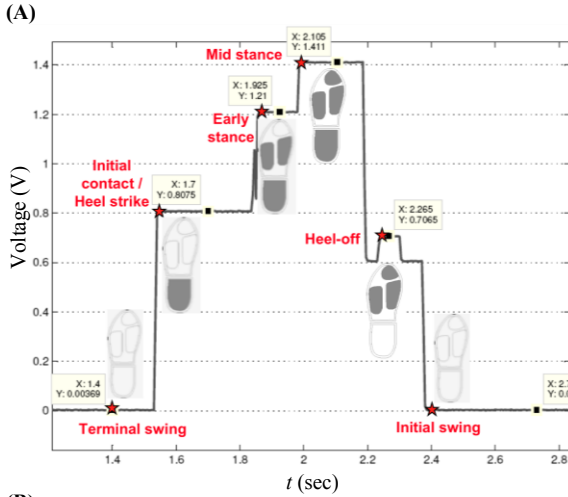


Fig. 3. (A) Footswitch trace during a typical gait cycle. Shaded regions within the footprints represent instants when one or more switches close due to the occurrence of gait event(s) (filled asterisks); (B) Block diagram of the event-triggered, sub-task control system. The event of interest shown is heel-off (dashed lines, shaded row in event table) [12].

II. A BIOMECHANICAL MODEL OF PUSH-OFF PROPULSION

A. Notations and definitions

For arbitrary segment angles, $x_i, y_i \in \mathfrak{R}$, we denote operators $S: \mathfrak{R} \rightarrow [0,1]$, $C: \mathfrak{R} \rightarrow [0,1]$ as $S_i = \sin x_i$, $C_i = \cos x_i$; $S_{x \pm y} = \sin(x \pm y)$; $\Delta x_{ij} = x_j - x_i$ ($i \neq j$); $S'_i = \sin(x_i - x_i(0))$, $C'_i = \cos(x_i - x_i(0))$ where $x_i(0) = x_i(t)|_{t=0}$. In what follows, M is total mass (body mass m_b plus foot mass m_f); H is total height (body linkage length, L plus foot height, y_a); (x_a, y_a) is ankle position from forefoot; l_f is ankle distance from forefoot; r_f is foot center-of-mass (COM) distance from forefoot; c_a is foot COM horizontal position from ankle; I_f and I_a are foot moment of inertia (MOI) about COM and about ankle respectively; I_b is body MOI, so that body MOI about ankle is $I_b + m_b r_b^2$; and subscripts “1” (or “a”) and “2” (or “b”) refer to ankle joint and body, respectively; and P_x^+ denotes MTS A-P positive propulsive impulse. Other variables are defined in the

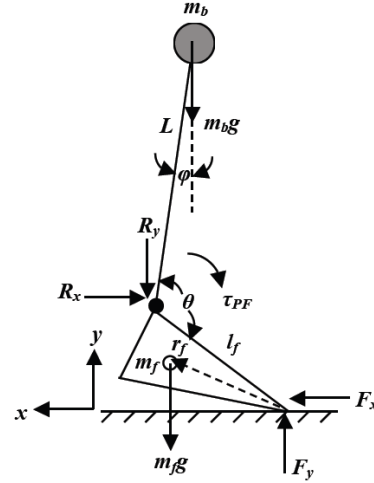


Fig. 4. Schematic of a 2-segment, sagittal-plane inverted pendulum model during terminal stance. The body COM is anterior to vertical with foot (except toe) off the ground. Anklebot PF assistance provides supplemental PF propulsion during this period to alleviate impaired pre-swing push-off deficits. A step-function waveform with duration $t_{HO} \leq t < t_{TO}$ and peak angle θ_{PF}^* is commanded during assisted gait (Section II-B). In the figure, F_x, F_y : A-P and vertical GRF, τ_{PF} : robot torque, φ : body angle with respect to vertical, θ : ankle angle; R_x, R_y : horizontal and vertical reaction forces acting on the ankle.

sections below as development of the model evolves.

B. Model description

We consider a sagittal-plane, 2-segment inverted pendulum (IP) model of the human “body” (head-arm-trunk plus leg minus foot) with the massless linkage acting as pivot over a moving base of support (BOS) i.e., foot (Fig. 4-A). The body mass is assumed to be concentrated as a point mass (m_b) on the distal end of the linkage with length L . The foot including ankle joint, is a separate rigid body with mass (m_f) located at the foot COM. To derive a model for propulsion dynamics, we assume a body posture at the instant of terminal stance—i.e., the body COM is slightly anterior to the vertical (representing forward COM momentum) with the foot (except toe) above the BOS.

C. Statements of the problem and equations of motion

The problem to be solved is as follows: given a subject’s body height (H), mass (M), and steady-state self-selected walking speed (s), determine: a) P_x^+ (output, N-s) resulting from a given value of K (input, Nm/rad); and b) minimum robot stiffness (input K_{min} , Nm/rad) needed to generate desired (e.g., normative) P_x^+ (output, N-s); mathematically,

$$K_{min} = \{K : P_x^+ \geq P_d\}, \quad (1)$$

where P_x^+ and P_d are the actual and desired peak propulsive impulses during MTS, respectively i.e.

$$P_x^+ := \int_{t^+} |\bar{F}_x| dt, \quad (2)$$

and t^+ are time epochs of positive impulse when A-P GRF > 0 (in contrast to braking impulse when A-P GRF < 0) i.e.

$$t^+ = \{t \in [t_{HO}, t_{TO}]: \vec{F}_x > 0\} \quad (3)$$

where t_{HO} and t_{TO} denote instants of heel-off (characterized by opening of heel switch with the medial, lateral and forefoot switches closed) and toe-off (characterized by opening of all individual foot switches) respectively, so that $[t_{HO}, t_{TO})$ represents MTS duration. To reiterate, both models will link a key Anklebot parameter (K) to a key gait function output (P_x^+). To formulate model dynamics, we initially use segment angles from horizontal as generalized coordinates with x-axis directed toward posterior of the foot (Fig. 4), with θ_1 and θ_2 representing the ankle angle and body angle from horizontal, respectively; additionally, $\theta_1' \approx \theta_1 - \theta_1(t=0)$ represents the angle of foot COM from horizontal. Then, the kinetic (T) and potential (V) energies of the segments are given by

$$T = \frac{1}{2}(I_f + m_f r_f^2 + m_b l_f^2) \dot{\theta}_1^2 + \frac{1}{2}(I_b + m_b r_b^2) \dot{\theta}_2^2 + m_b l_f r_b \dot{\theta}_1 \dot{\theta}_2 C_{12} \quad (3)$$

$$V = [m_f r_f S_1' + m_b (l_f S_1 + r_b S_2)] g, \quad (4)$$

with $S_1 = \sin \theta_1$, $C_1 = \cos \theta_1$, $S_{12} = \sin \Delta \theta_{21}$, $C_{12} = \cos \Delta \theta_{21}$, $S_1' = \sin(\theta_1 - \theta_1(t=0))$, and $\Delta \theta_{21} = \theta_2 - \theta_1$ as defined by convention. Using Lagrangian formulation, the dynamic equations of the model are obtained as:

$$\tau = M_1 \ddot{\theta}_1 + M_{12} (\ddot{\theta}_2 C_{12} - \dot{\theta}_2^2 S_{12}) + (m_f r_f C_1' + m_b l_f C_1) g \quad (5)$$

$$-\tau = M_2 \ddot{\theta}_2 + M_{12} (\ddot{\theta}_1 C_{12} + \dot{\theta}_1^2 S_{12}) + (m_b r_b C_2) g \quad (6)$$

where

$$M_1 = I_f + m_f r_f^2 + m_b l_f^2, \quad (7)$$

$$M_2 = I_b + m_b r_b^2, \quad (8)$$

$$M_{12} = m_b l_f r_b. \quad (9)$$

Next, these equations are transformed into natural coordinates (θ , φ) via the following transformations:

$$\theta_1 = \theta + \varphi - 90^\circ, \quad \theta_2 = \varphi + 90^\circ, \quad (10)$$

$$\dot{\theta}_1 = \dot{\theta} + \dot{\varphi}, \quad \dot{\theta}_2 = \dot{\varphi}, \quad (11)$$

$$\ddot{\theta}_1 = \ddot{\theta} + \ddot{\varphi}, \quad \ddot{\theta}_2 = \ddot{\varphi}, \quad (12)$$

$$C_{\theta_1} = S_{\theta+\varphi}, \quad S_{\theta_1} = -C_{\theta+\varphi}, \quad C_{\theta_2} = -S_\varphi, \quad S_{\theta_2} = C_\varphi. \quad (13)$$

The dynamics in Eqs. (5) and (6) can now be written as

$$\tau = M_1 \ddot{\theta} + (M_1 - M_{12} C_\theta) \ddot{\varphi} - M_{12} \dot{\varphi}^2 S_\theta + (m_f r_f S_{\theta+\varphi} + m_b l_f S_{\theta+\varphi}) g \quad (14)$$

$$-\tau = M_{12} C_\theta \ddot{\theta} + (M_2 - M_{12} C_\theta) \ddot{\varphi} + (\dot{\theta} + \dot{\varphi})^2 S_\theta - (m_b r_b S_\varphi) g. \quad (15)$$

To compute GRFs, we use d'Alembert's principle to obtain

$$F_x = m_f a_{f,x} + m_b a_{b,x}, \quad (16)$$

$$F_y = (m_b + m_f) g + m_b a_{b,y} + m_f a_{f,y}, \quad (17)$$

where the components of foot and body COM accelerations are computed using the following expressions:

$$a_{f,x} = r_f (\ddot{\theta} + \ddot{\varphi}) C_{\theta+\varphi-\psi} - r_f (\dot{\theta} + \dot{\varphi})^2 S_{\theta+\varphi-\psi}, \quad (18)$$

$$a_{f,y} = r_f (\ddot{\theta} + \ddot{\varphi}) S_{\theta+\varphi-\psi} + r_f (\dot{\theta} + \dot{\varphi})^2 C_{\theta+\varphi-\psi}, \quad (19)$$

$$a_{m,x} = l_f (\ddot{\theta} + \ddot{\varphi}) C_{\theta+\varphi} - l_f (\dot{\theta} + \dot{\varphi})^2 S_{\theta+\varphi} - r_b (\ddot{\varphi} C_\varphi - \dot{\varphi}^2 S_\varphi), \quad (20)$$

$$a_{m,y} = l_f (\ddot{\theta} + \ddot{\varphi}) S_{\theta+\varphi} + l_f (\dot{\theta} + \dot{\varphi})^2 C_{\theta+\varphi} - r_b (\ddot{\varphi} S_\varphi + \dot{\varphi}^2 C_\varphi). \quad (21)$$

To relate the GRF to ankle torque, we consider the foot as it pivots around the ankle (Fig. 4-B) and its dynamic equation:

$$\tau_a = I_a (\ddot{\theta} + \ddot{\varphi}) + l_f (F_x C_{\theta+\varphi} + F_y S_{\theta+\varphi}) - m_f g c_a. \quad (22)$$

where $\tau_a = \tau_h + \tau_{PF}$ is the net torque at the ankle, comprised of the human (τ_h) and robot (τ_{PF}) torques. Using methods described in Section-III, we “baseline subtract” the unassisted human torque ($\tau_{h,K=0}$), so that $\tau_a = \tau_a - \tau_{h,K=0} \approx \tau_{PF}$. Then, we swap τ_a in Eq. (22) with

$$\tau_{PF} = K(\theta^* - \theta) + b(\dot{\theta}^* - \dot{\theta}), \quad (23)$$

where $\theta^* = \theta_{PF}^*$ and $\dot{\theta}^* = 0$, to obtain

$$K\theta_{PF}^* - K\theta - b\dot{\theta} = I_a (\ddot{\theta} + \ddot{\varphi}) + l_f (F_x C_{\theta+\varphi} + F_y S_{\theta+\varphi}) - m_f g c_a. \quad (24)$$

D. Linking propulsion dynamics to robotic support

To calculate the MTS A-P propulsive impulse, we integrate Eq. (24) from t_{HO} to t_{TO^-} and rearrange to obtain:

$$K(\theta_{PF}^* \Delta T_{LS} - I_\theta) = I_a (\dot{\theta} + \dot{\varphi}) \Big|_{t_{HO}}^{t_{TO^-}} + l_f \int_{t_{HO}}^{t_{TO^-}} (F_x C_{\theta+\varphi} + F_y S_{\theta+\varphi}) dt - b \Delta \theta_{LS} - m_f g c_a \Delta T_{LS}. \quad (25)$$

where $\Delta T_{LS}(s, K) = t_{TO^-} - t_{HO}$ is LS duration (a proxy for

gait speed) with $t_{TO^-} = \lim_{\delta \rightarrow 0^+} t_{TO} - \delta$, $I_\theta(s, K) = \int_{t_{HO}}^{t_{TO^-}} \theta(t, K) dt$

is ankle angle vs. time area-under-curve (AUC), and $\Delta \theta_{LS}$ is the ankle angular displacement from t_{HO} to t_{TO^-} . The first term of the RHS of Eq. (25) may now be written as

$$(\dot{\theta} + \dot{\varphi}) \Big|_{t_{HO}}^{t_{TO^-}} = \Delta \dot{\theta} + \Delta \dot{\varphi}, \quad (26)$$

where $\Delta \dot{\theta}(s, K)$ and $\Delta \dot{\varphi}$ are difference in ankle and body angular velocities from heel-off to toe-off, respectively. Substituting Eq. (26) into (25) and rearranging, we obtain

$$l_f \int_{t_{HO}}^{t_{TO}^-} (F_x C_{\theta+\phi} + F_y S_{\theta+\phi}) dt = K(\theta_{PF}^* \Delta T_{LS} - I_\theta) - I_a(\Delta\dot{\theta} + \Delta\dot{\phi}) + b\Delta\theta_{LS} + m_f g c_a \Delta T_{LS}. \quad (27)$$

Note that our desired output variable P_x^+ does not explicitly appear in LHS of Eq. (27). To proceed further, consider that

$$|F_x C_{\theta+\phi}| \leq |F_x|, |F_y S_{\theta+\phi}| \leq |F_y|, \forall t \in D = [\sigma_1, \sigma_2],$$

for arbitrary bounded domain $D = [\sigma_1, \sigma_2]$. Moreover, since $|F_y S_{\theta+\phi}|$ and $|F_x C_{\theta+\phi}|$ are both Riemann-integrable (bounded and continuous everywhere), we can use the following general inequality property:

$$\int_D |F_x C_{\theta+\phi}| dt \leq \int_D |F_x| dt = P_x^+, \quad (28)$$

$$\int_D |F_y S_{\theta+\phi}| dt \leq \int_D |F_y| dt. \quad (29)$$

Therefore, the integral term in LHS of Eq. (27) reduces to

$$\int_{t_{HO}}^{t_{TO}^-} (F_x C_{\theta+\phi} + F_y S_{\theta+\phi}) dt \leq P_x^+ + \int_{t_{HO}}^{t_{TO}^-} |F_y| dt. \quad (30)$$

Using inequality in (30) and Eq. (27), and rearranging, we obtain a nonlinear inequality between K and P_x^+ , given by

$$P_x^+ \geq \{K(\theta_{PF}^* \Delta T_{LS} - I_\theta) - I_a(\Delta\dot{\theta} + \Delta\dot{\phi}) + b\Delta\theta_{LS} + m_f g c_a \Delta T_{LS} - l_f \int_{t_{HO}}^{t_{TO}^-} |F_y| dt\} / l_f. \quad (31)$$

The minimum stiffness, K_{min} needed to achieve $P_x^+ \geq P_d$ can be obtained by imposing the condition of Eq. (1) in (31):

$$K(\theta_{PF}^* \Delta T_{LS} - I_\theta) - I_a(\Delta\dot{\theta} + \Delta\dot{\phi}) + b\Delta\theta_{LS} + m_f g c_a \Delta T_{LS} \geq l_f (P_d + \int_{t_{HO}}^{t_{TO}^-} |F_y| dt). \quad (32)$$

Note that inequality (33) is nonlinear in K (since ΔT_{LS} , I_θ , $\Delta\theta_{LS}$ etc. vary with K) and can be computed numerically for given P_d (see model simulation in Fig. 9-A). Inequalities (31) and (32) are *two variants of the desired model*: Inequality (31) predicts MTS A-P positive propulsive impulse, P_x^+ for inputs robot stiffness, K . Inequality (32) may be used to solve for the minimum stiffness, K_{min} needed for MTS A-P positive propulsive impulse to be equal to or greater than a desired value (e.g., normative), P_d . In the remainder of the article, we will validate the first variant of the model by comparing its predictions to experimental data.

E. Calculating model constants

The push-off propulsion model given by inequality (32) consists of a number of constants that need to be calculated. Each constant (except robot damping, b) can be classified as either: 1) individual whole-body (e.g., H , M) or ankle joint (e.g., x_a , y_a , c_a , m_f , I_a) dimensions that are independent of K ; or 2) gait characteristics (e.g., $\Delta\theta_{LS}$, I_θ , ΔT_{LS}) that are dependent on K ; or 3) reference parameters (e.g., θ_{PF}^*) that

are independent of K . To validate the model, these constants are calculated using body mass and height, joint dimensions relative to body mass and height [16,17], and force plate data acquired during unassisted gait (see Section IV).

III. EXPERIMENTS

We computed the A-P propulsive impulses from dual force plate (Bertec, Columbus OH) GRF data collected during floor walking (averaged across 3 trials) at self-selected comfortable speed. The force plate data consisted of raw GRF time series in the Cartesian coordinate system (X : anterior-posterior, Y : vertical, Z : medial-lateral). Two sets of trials were conducted: the first set was with the Anklebot in a “record-only” mode, to acquire unassisted GRFs and calculate volitional (human only) propulsive impulse. The second set of trials consisted of walking with Anklebot PF assistance at 5 stiffness settings ($K = 50$ N-m/rad to 250 N-m/rad in increments of 50 N-m/rad). During these trials, the Anklebot provided PF assistance, commencing at heel-off and peaking just prior to toe-off. Heel-off was detected by the footswitch (Fig. 5-A) when the voltage dropped from ~ 1.5 V (full-load) to ~ 0.7 V (forefoot + toe switches closed). The difference between unassisted and assisted A-P propulsion was calculated to approximate the propulsive impulse due to the robot alone². Throughout, the commanded peak PF angle was held constant at $\theta_{PF}^* = 20^\circ$.

The A-P propulsion impulse was numerically computed from unfiltered GRF traces using a custom MATLAB[®] program: first, the vertical ground reaction force (F_y) vector was used to identify mid stance (i.e., when F_y is at a local maximum, the leg is fully loaded) and terminal stance (i.e., when F_y first equals 0, the leg is fully unloaded) events (Fig. 5-B). Second, within the MTS phase, the time epochs during which $F_x > 0$ are identified to extract positive impulses. Finally, the time integral (trapezoidal method) $F_x > 0$ components during MTS period yield P_x^+ (Fig. 5-C).

IV. RESULTS

A. Subject

A healthy 18-year old adult participated in the experiments. The subject gave informed consent prior to participation. Subject anthropometry is listed in Table I.

B. Model simulations, and validation

Figure 5-D shows exemplar unassisted ($K = 0$ N-m/rad) and assisted ($K = 50$ N-m/rad) traces of MTS A-P GRF. Using methods described previously, we computed the propulsion due to robot alone (assisted minus unassisted), at each K . For model validation, the constants (Table I) were calculated from footswitch traces and robot-measured ankle

²Since torque from human muscle was not measured, we assume same muscle activation levels at different stiffnesses, i.e., $\tau_h \approx \tau_{h,K=0}$. We acknowledge the simplistic nature of this assumption; however, it enables a basic experiment to validate the model as a first pass by attributing the torque difference solely to robot stiffness, i.e., $\tau_a \approx \tau_{PF}$.

kinematics during unassisted walking over force plates (Fig. 6). Table II shows key model constants across the selected stiffness range with constant damping, $b = 1$ N-m-s/rad. These are used in inequality (31) to yield P_x^+ for each K .

TABLE I
SUBJECT WHOLE-BODY, ANKLE JOINT, AND “UPPER BODY”
ANTHROPOMETRIC DATA

Parameter, Symbol	Value (SI Units)
Body height, H	1.78 (m)
Body mass, M	75 (kg)
Body linkage length*, L	1.73 (m)
Body (minus foot) mass, m_b	74 (kg)
Foot mass, m_f	1.0 (kg)
Ankle distance from forefoot, l_f	0.215 (m)
Ankle (X,Y) coordinates from forefoot (x_a, y_a)	(0.2, 0.075) (m)
Foot COM horizontal distance from ankle, c_a	0.035 (m)
Foot COM distance from forefoot, r_f	0.167 (m)
Foot moment of inertia, I_f	8×10^{-3} (kg-m ²)
Foot moment of inertial about ankle, I_a	10^{-2} (kg-m ²)
Body COM to ankle distance, r_b	1.0 (m)
Body moment of inertia about COM, I_b	12.66 (kg-m ²)
Body moment of inertia about ankle, $I_b + m_b r_b^2$	87.66 (rad-sec)

*Computed using [15,16] relative to body mass (M) and height (H).

Figure 7 shows 3 key model constants in Table II as a function of robot stiffness, K . Our findings are that higher stiffness results in: a) lower late stance durations (ΔT_{LS}), with a nonlinear inverse-Sigmoid type ΔT_{LS} vs. K trend; b) smaller ankle angle AUC (I_θ), with a positive linear I_θ vs. K trend; and c) lower vertical GRF AUC ($\int F_y dt$), with a constant-ramp down $\int F_y dt$ vs. K trend; and vice versa.

Figure 8-A shows predicted vs. actual propulsive impulses normalized to body mass, across all 5 values of K , the former calculated using model constants in Table II. The average model-predicted values (0.71 ± 0.11 N-s/kg) were within 10% of the experimental values (0.64 ± 0.11 N-s/kg) across the full range of $K = 50$ to 250 Nm/rad. The absolute errors were 0.074 ± 0.067 N-s/kg across the full range of K , with lower values (0.043 ± 0.034 N-s/kg) for $K \leq 150$ N-m/rad and relatively higher errors (0.121 ± 0.93 N-s/kg) for $K \geq 200$ Nm/rad. Figure 8-B shows 3D simulation of minimum stiffness (K_{min}) vs. desired propulsive impulse (P_d) vs. late stance duration (ΔT_{LS}), for arbitrarily chosen model constant set $\{\Delta\theta_{LS} = -0.57$ rad, $\Delta\dot{\theta} = 0.28$ rad/s, $I_\theta = -0.14$ rad-s, $\int F_y dt = 68.2$ N-s}. As expected, the model correctly predicts that slower walking speeds (i.e., higher ΔT_{LS}) necessitates greater K to achieve a given P_d , and vice versa.

TABLE II
MODEL CONSTANTS FOR EACH STIFFNESS VALUE

Stiffness, K (Nm/rad)	ΔT_{LS} (sec)*	$\Delta\theta_{LS}$ (rad)**	$\Delta\dot{\theta}$ (rad/s)**	I_θ (rad-s)**	$\int F_y dt$ (N-s)*
50	0.1552	-0.5763	0.2867	-0.1391	68.186
100	0.1581	-0.0730	0.0771	-0.0959	68.919
150	0.1496	-0.2314	0.1092	-0.0601	68.107
200	0.1306	-0.4009	0.2578	-0.0624	56.624
250	0.1282	-0.8981	0.6885	-0.0397	49.572

*Calculated using foot switch time series, and Anklebot-recorded angle and angular velocity time series. **Calculated from vertical GRF time series. Integral term numerically computed using MATLAB® “trapz” function.

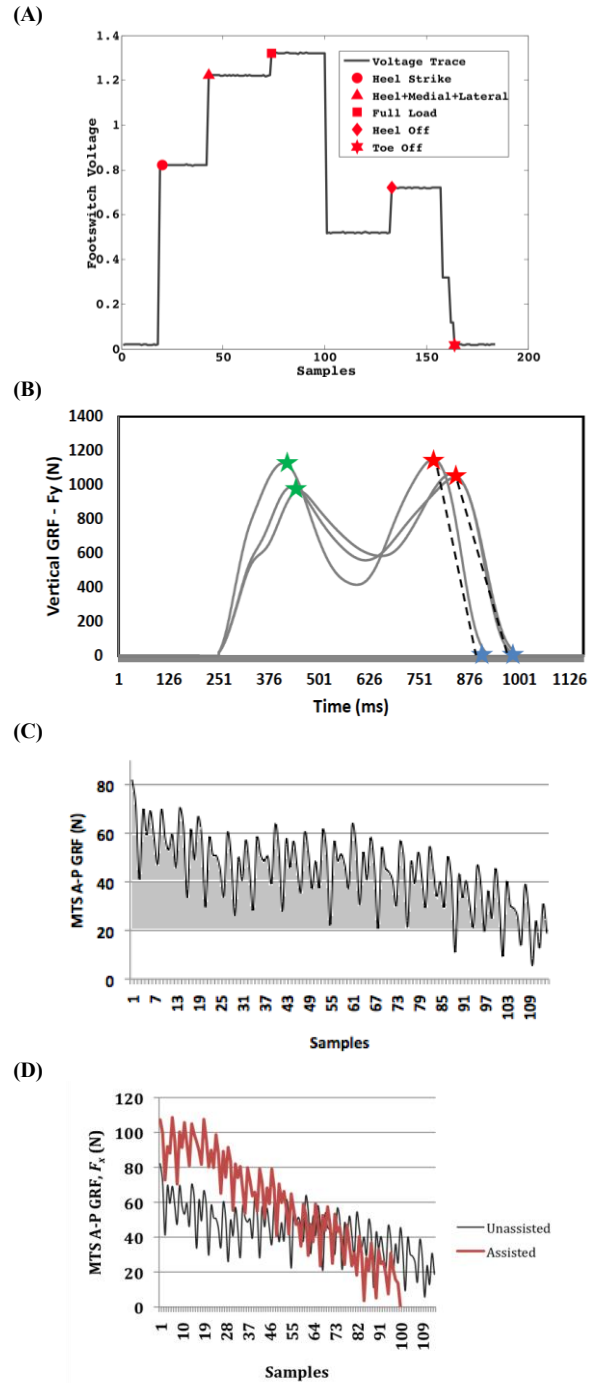


Fig. 5. (A) Footswitch voltage trace of a single gait cycle during unassisted walking over force plates at self-selected comfortable speed. The plot shows heel-strike, mid-stance (full load), and toe-off sub-events. Late stance is defined as the duration between heel-off and toe-off. During assisted trials, the Anklebot provides PF torque during this period to enhance push-off propulsion; (B) Unassisted vertical GRF time profiles collected from force plates during 3 trials of walking. The biphasic traces show heel strike (green asterisk), mid stance (red asterisk) and start of swing (blue asterisk). These time points are used to identify MTS; (C) Exemplar unassisted MTS A-P GRF ($t=0$ is mid-stance). The shaded region is the area under the curve, i.e., the integral of GRF or, positive propulsive impulse; (D) Exemplar unfiltered traces of MTS A-P GRF collected from force plate during assisted and unassisted floor walking ($t=0$ is mid-stance). A key model constant, $\int F_y dt$ is calculated from these data.

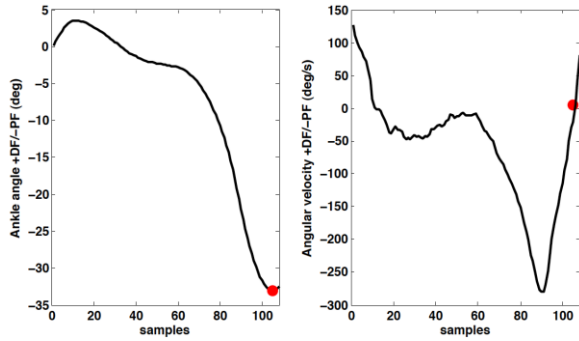


Fig 6. Exemplar ankle angle (*left*) and angular velocity (*right*) time series during unassisted ($K = 0$ Nm/rad) record-only walking. The traces are shown only for the MTS period, i.e., $t=0$ represents heel-off and filled circles represent toe-off. Four out of five model constants (ΔT_{LS} , $\Delta \theta_{LS}$, $\Delta \dot{\theta}_{LS}$, I_0) are computed from these data.

C. Comparison to existing literature

The effect of leg propulsion on walking speed and its relationship to muscle activity has been widely studied (e.g., [4,5,7,18]). However, none of those investigations deployed robotics for PF gait therapy. Hence, a direct comparison cannot be made between findings from those studies and those reported here. Still, the predicted values of A-P positive impulse during the MTS epoch reported here are much higher than those reported elsewhere, e.g., [18] for healthy subjects (0.165 to 0.272 N-s/kg, $n=21$). The primary reason for this is that unlike those studies, here we report impulses resulting from an actuated device. In addition, there are other differences: 1) Experimental conditions: for example, in [18] control (able-bodied) subjects walked over split-belt TM without any robotic device vs. over ground with supplemental robotic assistance and unilateral robot mass loading condition in our study; and 2) Subject demographics: older nondisabled subjects (65.2 ± 9.6 yrs.) in [18] vs. a young healthy (18 yr. old) subject in this study.

V. CLINICAL AND REHABILITATION RELEVANCE

The push-off model developed here and those in our previous work (swing, landing) [12] are meant to predict reasonable initial values (“look-up” table) for appropriate robotic assistance for individual HP gait deficits during Anklebot-assisted walking. Moreover, the model predictions may also be used to systematically progress robotic support over an intervention concomitant with recovery, an approach consistent with our previous studies (e.g., [9,12]). In control terms, these models inform us of the controller gains (K and/or b) needed for deficit-adjusted robotic gait therapy. In [12] we reported the minimum stiffness needed for desired swing assist ($K_{min,swing}$) and the minimum damping needed for constraining landing forces ($b_{min,land}$) to desired levels. Those limits yielded a deficit-based map in the controller space [12]—the push-off model adds another piece to that map by linking robotic assistance to push-off impulse (Fig. 9). Note that, in practice, the robot stiffness predicted by two of these models—enhanced swing clearance [12] and push-

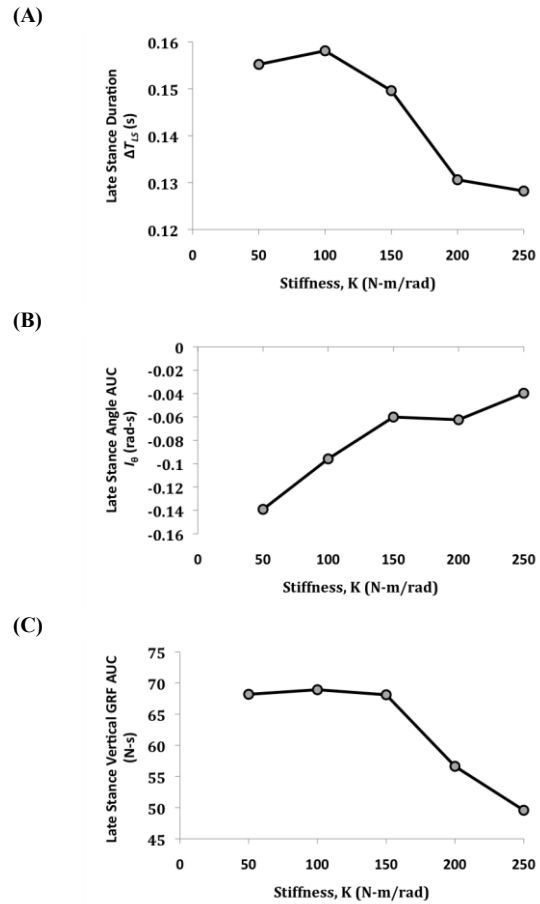


Fig. 7. Variation of key model constants with stiffness, K : (A) Late stance duration (ΔT_{LS}); (B) Late stance angle AUC (I_0); and (C) Late stance vertical GRF AUC $\int F_y dt$.

off propulsion, needs to be intersected with the achievable Anklebot impedance ranges³ [8] to prevent instability, i.e.,

$$K = [K_{min}, \infty) \cap (0, K(b)_{max,stab}) = [K_{min}, K(b)_{max,stab}) \quad (33)$$

VI. CONCLUSIONS, STUDY LIMITATIONS AND FUTURE WORK

A sagittal-plane model for mid-to-terminal stance A-P propulsion dynamics for assisted walking is developed. The model is a 1st step toward calibrating and parameterizing the Anklebot support, by predicting reasonable initial values of robotic assist for desired A-P propulsion during Anklebot-assisted gait. The model incorporates individual whole-body and (ankle) joint anthropometry similar to other biomechanical models (e.g., [17]), as well as temporal-distance kinematics and kinetics of unassisted and assisted over ground walking. Initial validation tests verified that the model can predict A-P propulsive impulses with reasonable accuracy across a wide range of stiffness values. We acknowledge the limitation of a “single subject” experiment—clearly, model validity needs to be more broadly established. Hence, future work will focus on: (a)

³Characterized by K - b uncoupled stability curve [8] that is derived by measuring the highest K attainable at a given b before instability (persistent non-decaying oscillations) occurs ($K(b)_{max,stab}$), across a range of values of b .

validating the model in a larger cohort of able-bodied adults to serve as referent population and in subjects with stroke with varying levels of force generating-impairments; and (b) analysis of the forward translation of the body center of gravity (total amount, velocity of CoP progression in sagittal and lateral directions) as well as 3D gait analysis of the proximal joints, especially at the level of the knee joint given its contribution to push-off through hyperextension thrust.

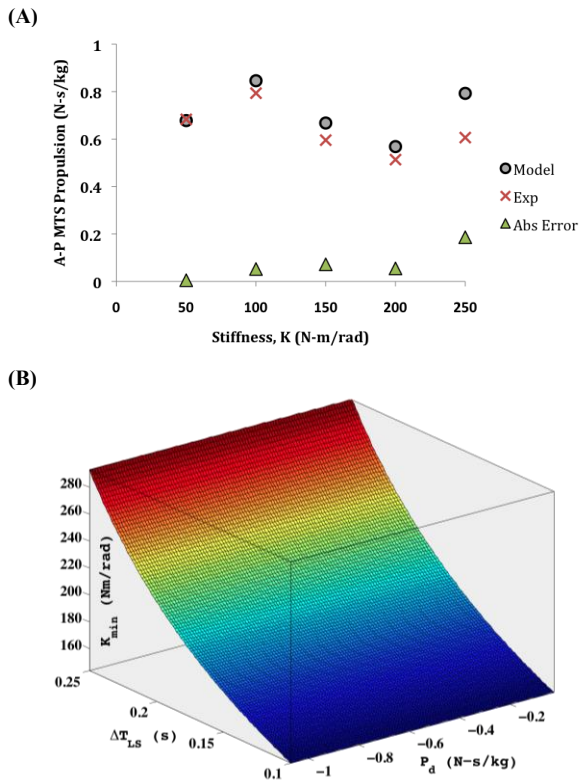


Fig. 8. Model validation and simulations. (A) Comparison of model vs. actual A-P MTS positive propulsive impulse for 5 values of stiffness, K . Also shown in the plot are the absolute values of the model vs. experiment residuals, which are “small” demonstrating accuracy of this first form model; and (B) 3D plot showing nonlinear relationship of minimum stiffness (K_{min} , Z-axis) as a function of desired propulsion (P_d , X-axis) and late stance duration (ΔT_{LS} , Y-axis).

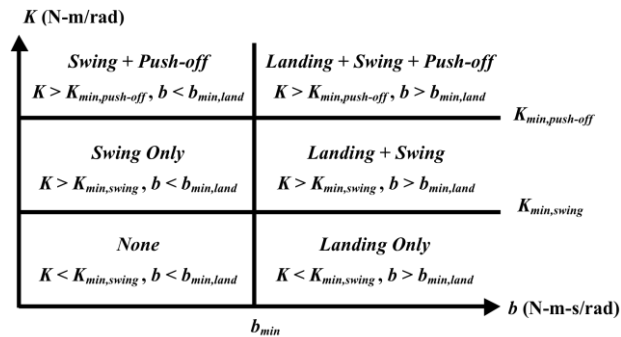


Fig. 9. Deficit-based map in the controller parameter (K - b) plane. The map is an extension to that reported in [12] by incorporating the push-off model. Depending on the type of gait deficit being targeted, reasonable values of K and/or b can be chosen for desired performance.

REFERENCES

- [1] Heart disease and stroke statistics: American Heart Association; 2009. Available from: www.americanheart.org/statistics.
- [2] A. Forster and J. Young, “Incidence and consequences of falls due to stroke: A systematic inquiry,” *BMJ*, vol. 311, pp. 83-6, 1995.
- [3] T.P. Andriacchi, J.A. Ogle, and J.O. Galante, “Walking speed as a basis for normal and abnormal gait measurements,” *J Biomech*, vol. 10, pp. 261-68, 1977.
- [4] M.G. Bowden, C.K. Balasubramanian, R.R. Neptune, and S.A. Kautz, “Anterior-posterior ground reaction forces as a measure of paretic leg contribution in hemiparetic walking,” *Stroke*, vol. 37, pp. 872-76, 2006.
- [5] L.J. Turns, R.R. Neptune, and S.A. Kautz, “Relationships between muscle activity and anteroposterior ground reaction forces in hemiparetic walking,” *Arch Phys Med Rehabil*, vol. 88, pp. 1127-35, 2007.
- [6] J. Perry, M. Garrett, J.K. Gronley, and S.J. Mulroy, “Classification of walking handicap in the stroke population,” *Stroke*, vol. 26, pp. 982-89, 1995.
- [7] R.R. Neptune, S.A. Kautz, and F.E. Zajac, “Contributions of the individual ankle plantar flexors to support, forward progression and swing initiation during walking,” *J Biomech*, vol. 34, pp. 1387-98, 2001.
- [8] A. Roy, H.I. Krebs, D.J. Williams, C.T. Bever, L.W. Forrester, R.F. Macko, and N. Hogan, “Robot-aided neurorehabilitation: A novel robot for ankle rehabilitation,” *IEEE T Rob*, vol. 25, pp. 569-82, 2009.
- [9] L.W. Forrester, A. Roy, H.I. Krebs, and R.F. Macko, “Ankle Training With a Robotic Device Improves Hemiparetic Gait After a Stroke,” *Neurorehabil Neural Repair*, vol. 25, pp. 369-77, 2011.
- [10] L.W. Forrester, A. Roy, A. Krywonis, G. Kehs, H.I. Krebs, and R.F. Macko, “Modular Ankle Robotics Training in Early Sub-Acute Stroke: A Randomized Controlled Pilot Study,” *Neurorehabil Neural Repair*, 2014 (In-Press, Feb 2014). DOI: 10.1177/1545968314521004.
- [11] T.G. Hornby, D.D. Campbell, and J.H. Kahn, “Enhanced gait-related improvements after therapist- versus robotic-assisted locomotor training in subjects with chronic stroke: a randomized controlled study,” *Stroke*, vol. 39, pp. 1786-92, 2008.
- [12] A. Roy, H.I. Krebs, J.E. Barton, R.F. Macko, and L.W. Forrester, “Anklebot-Assisted Locomotor Training After Stroke: A Novel Deficit-Adjusted Control Approach,” In: *Proc IEEE Int Conf Robotics and Automation (ICRA)*, Karlsruhe, Germany, pp. 2167-2174, 2013.
- [13] H.I. Krebs, J.J. Palazzolo, L. Dipietro, M. Ferraro, J. Krol, K. Ranneklev, B.T. Volpe, and N. Hogan, “Rehabilitation Robotics: Performance-based Progressive Robot-Assisted Therapy,” *Autonomous Robots*, Kluwer Academics vol. 15, pp. 7-20, 2003.
- [14] S.J. Olney and D.A. Winter, “Predictions of knee and ankle moments of force in walking from EMG and kinematic data,” *J Biomech*, vol. 18, pp. 9-20, 1985.
- [15] V. Zatsiorsky and V. Seluyanov, “The mass and inertia characteristics of the main segments of the human body,” In: *Biomechanics* (Eds. Matsui, H., Kobayashi, K.), 1152-59. Human Kinetic, Illinois, 1983.
- [16] W. T. Dempster and G. R. L. Gaughran, Properties of Body Segments Based on Size and Weight, *Am J Anatomy*, vol.120, pp. 33-54, 1967.
- [17] K. Iqbal and A. Roy, “A novel theoretical framework for the dynamic stability analysis, movement control, and trajectory generation in a multisegment biomechanical model,” *J Biomech Eng*, vol. 131, pp. 011002, 2009.
- [18] C.L. Peterson, J. Cheng, S.A. Kautz, and R.R. Neptune, “Leg extension is an important predictor of paretic leg propulsion in hemiparetic walking,” *Gait Posture*, vol. 32, pp. 451-56, 2010.